VOL. 20, NO. 18, SEPTEMBER 2025 ISSN 1819-6608
ARPN Journal of Engineering and Applied Sciences

www.arpnjournals.com

AERODYNAMICS STUDY ON SLAT AND FLAP EMBEDMENT ONTO A FLAT PLATE FOR HIGH ALTITUDE PLATFORM UAV APPLICATION

Alias M. S.[1], Mohd Rafie A. S.[1], Abdul Hamid M. F.[1], Gires E.[1] and Mohd Aris K. D.[2]
[1]Department of Aerospace Engineering, Faculty of Engineering, Universiti Putra Malaysia, Serdang, Selangor, Malaysia
[2]Aerospace Engineering Section, Universiti Kuala Lumpur Malaysian Institute of Aviation Technology, Dengkil, Selangor, Malaysia
E-Mail: m.shahidi@unikl.edu.my

ABSTRACT

The aerodynamic performance of Unmanned Aerial Vehicles (UAVs) is critical for optimizing lift, reducing drag, and achieving efficient flight across a range of wind speeds, for High Altitude Platforms (HAPs applications. This research investigates the effects of basic geometry shapes of flap and slat designs on aerodynamic performance, specifically targeting enhancements in lift-to-drag ratio at various air velocities of 5, 10, 15, and 20 ms^{-1} with 6 configurations of angles of attack. Three basic shape designs, rectangular, triangular, and semi-circular, which were embedded onto a flat plate, were evaluated experimentally in an open loop wind tunnel. The results revealed that the triangular and semi-circular slats and flaps consistently provided higher aerodynamic performance compared to the rectangular design, particularly at higher velocities and angles of attack. Experimental results showed lift increased with air velocity, with the 0°-7°-20° configuration yielding the highest performance. The triangular design achieved the best C_L/C_D of 4.134 for an air velocity of 20 ms^{-1}. Additionally, the triangular and semi-circular design exhibited superior aerodynamic stability and efficiency, making it well-suited for high-speed operations. These findings underscore the critical role of basic shape geometry in improving UAV flight performance across a wide range of air velocities, contributing to reduced mechanical loads, lower power consumption, and lighter system designs for HAP applications.

Keywords: unmanned aerial vehicle, slat, flap, aerodynamic performance, lift coefficient, drag coefficient.

Manuscript Received 6 May 2025; Revised 10 December 2025; Published 30 December 2025

1. INTRODUCTION

A High-Altitude Platform (HAP) is a system operating at altitudes of 20-50 km, higher than commercial and military aircraft but below satellites [1]. HAPs include aerostats [2], airships, and UAVs and are deployed globally based on their mission needs, especially in areas where traditional infrastructure is challenging or cost-prohibitive. HAPs provide critical support for Earth observation, surveillance, disaster response, telecommunications, and scientific research by delivering persistent, cost-effective coverage over targeted regions with the flexibility for rapid deployment and relocation.

Designed with aerodynamic structures, solar-powered propulsion, and advanced communication technologies, HAPs are versatile aerospace systems. Today, solar-powered UAVs and tethered balloons equipped with sensors, cameras, and communication tools are popular HAPs, suitable for both stationary and mobile operations depending on mission requirements [1][2][3][4]. HAP technology is significant for government agencies, telecommunications companies, research institutions, and military organizations, all of which contribute to its development and operational deployment as illustrated in Figure-1. Previous studies on atmospheric characteristics would impact HAP design. Variations in altitude result in differing wind speeds and air quality, directly influencing the aerodynamic performance of lifting devices. At an altitude of 20 km, the average wind speed is approximately 12.2 ms^{-1} [5]. This underscores the importance of tailoring HAP designs to specific altitude conditions to optimize lift, stability, and overall aerodynamic efficiency.

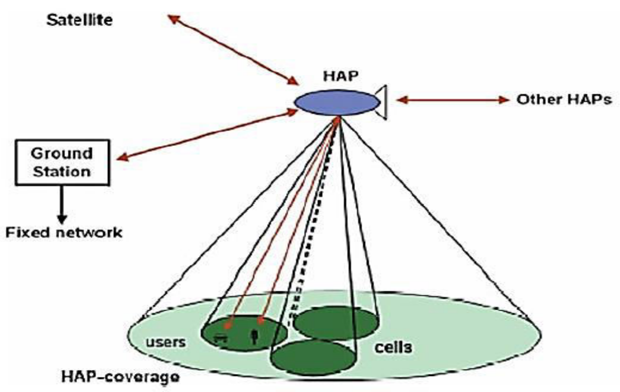

Figure-1. High-altitude platform diagram for telecommunication services [2].

Over the years, extensive research has focused on enhancing HAP's aerodynamic performance due to its critical impact on endurance, altitude capabilities, and overall mission effectiveness. The findings revealed that pressure buildup between the two rotating cylinders and the flat plate in the upper region generated a downward push force, which contributed to a reduction in lift and an increase in drag as air velocity increased along the CyFlap model's streamwise direction [6][7][8]. Additionally, maintaining the rotation of both cylinders required a significant power input. Determined by a similar concept,

 ISSN 1819-6608
ARPN Journal of Engineering and Applied Sciences

another research tackling low altitude application, which is AgroCyFlaP UAV, targets the significant issue of downwash in agriculture, which can disturb soil, plants, and surrounding materials. Initial results suggest that using the Magnus effect, the AgroCyFlaP can potentially reduce downwash by up to 90% [9]. However, further research is needed to refine its aerodynamics and ensure field viability. A key challenge is the high-power demand required for rotating cylinders at high speeds to maintain stability across different altitudes. While solar power is considered a sustainable energy source, it may not consistently meet these demands, particularly in critical operational conditions as illustrated in Figure-2.

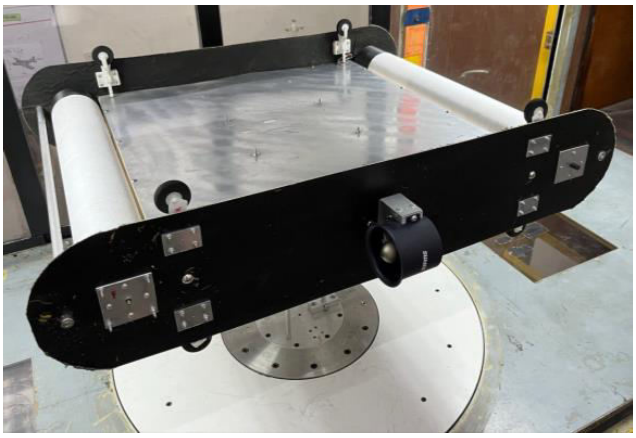

Figure-2. AgroCyFlaP UAV Experimental model [9].

Key aerodynamic factors such as lift, drag, and stability significantly impact a HAP UAV's endurance, flight efficiency, and operational capacity across various altitudes. Enhanced aerodynamic efficiency minimizes energy consumption, thus extending flight duration and enabling stable operation in challenging conditions. Improved aerodynamic performance also supports higher-altitude operations with better control and maneuverability, expanding the UAV's operations. Optimizing these factors is crucial for maximizing UAV effectiveness and mission success.

Slats and flaps are essential aerodynamic devices for airflow control, significantly enhancing lift and stability in varying flight conditions since their early application in the Wright Flyer 1 by Orville Wright in 1920 [10]. Slats, positioned at the leading edge, extend outward to create a gap, promoting smooth airflow over the wing at high angles of attack, thereby delaying stall and increasing lift. Flaps, located at the trailing edge, deflect downward to increase wing curvature, enhancing lift during takeoff and landing or increasing drag for controlled descent [10][11][12]. Together, slats and flaps optimize lift-to-drag ratios, ensuring aerodynamic efficiency across diverse operating conditions.

This study examines the influence of forward (slats) and rear (flaps) aerodynamic control surfaces on a blended wing body UAV to enhance airflow control and optimize performance [13]. In addition to improving lift and reducing drag, this approach aims to minimize mechanical load, power consumption, and overall UAV HAP system weight, thereby improving design efficiency. The research explores slat and flap configurations as potential alternatives to the AgroCyFlaP model, addressing its aerodynamic limitations at higher velocities. Experimental analyses will determine whether rectangular, triangular, and semi-circular designs can deliver comparable or superior lift-to-drag ratios and stability across various flight conditions.

2. METHODOLOGY

This research entailed an in-depth literature review, focusing on critical aerodynamic principles, aerodynamic characteristics, and performance implications of semi-active airflow control mechanisms, specifically through the integration of flap and slat. These airflow controls are embedded in the new design blended wing body (BWB) UAV for HAP application, functioning as a forward (FWD) section analogous to a slat and a rear (AFT) section acting as a flap.

Experimentally, a low-speed open-loop wind tunnel offers numerous advantages for aerodynamic experiments by creating a highly controlled environment [14]. This setup maintains consistent, predictable airflow, minimizing external influences that could impact data quality. By recirculating air, it operates with greater energy efficiency, reducing long-term costs compared to open-loop systems that require continuous air intake [15] [16]. The study presents a structured methodology for implementing an airflow control embedment onto a flat plate in experimental frameworks, with detailed descriptions provided in subsequent sections.

The geometries for both forward and rear air flow control (acting as slat and flap), as well as the flat plate model, were precisely defined and fabricated, taking into account the specifications of the Open-Loop Wind Tunnel (OLWT). The OLWT is commonly used for its cost-effectiveness and minimal spatial requirements, though it typically consumes more energy at a given speed than closed-circuit tunnels [17].

2.1 Geometry and Experimental Setup

The study incorporates forward and aft air flow control designs onto a flat plate, tailored to the Universiti Putra Malaysia OLWT's specifications, before model fabrication for experimental testing [17].

2.1.1 Design justification

The research work by H. Ali [7], inspired by the works of J. Wang [11] and T. Mueller [18] are recognized for their straightforward structure and historical importance in lift generation studies. A 1.00 m flat plate length from a previous study [7] was scaled down to a 1:0.6 ratio, taking into account both the payload zone within the flat plate of the intended Blended Wing Body HAP UAV and the specifications of the Open-Loop Wind Tunnel at Universiti Putra Malaysia [17].

ISSN 1819-6608
ARPN Journal of Engineering and Applied Sciences

www.arpnjournals.com

The semi-active airflow control, introduced as a primary control surface for the novel model, acts as an airflow separator, effectively extending the vortex wake for improved aerodynamic control [11]. The design includes three fundamental shapes optimized for simplicity and ease of production: rectangular, triangular, and semi-circle, selected based on comparative wind tunnel studies examining drag and lift coefficients for standard 2-D shapes [19]. Each design were tested with streamwise configurations relative to airflow as shown in Figures-3(a), 3(b) and 3(c): a FWD and AFT airflow control gap of 0.005D with length (L) of 0.2D, and a height (H) of 0.06D, adapted from J. Hwang's [11] and T. Mueller's [18] studies.

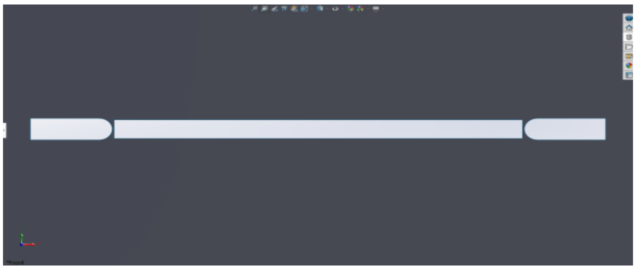

(a)

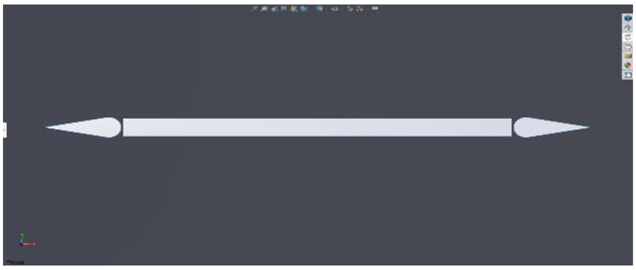

(b)

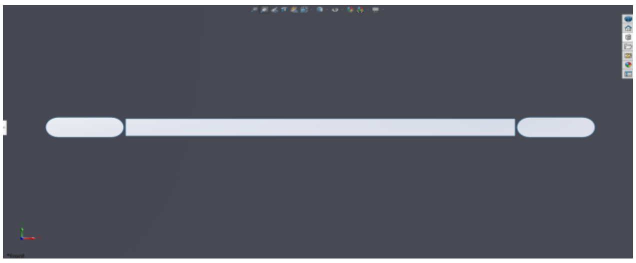

(c)

Figure-3. (a) Rectangular, (b) Triangular, and (c) Semi-Circular slat and flap embedment onto a flat plate.

2.2 Wind Tunnel Test Setup

Experimental methods in aerodynamics are essential for gaining insights into the interaction between airflow and objects such as aircraft, vehicles, and structures. These experiments focus on measuring and analyzing critical aerodynamic forces, including lift and drag, as well as assessing stability.

2.2.1 Experimental model fabrication

The design process for simple aerodynamic structures begins with the creation of three types of slat and flaps: semi-circular, triangular, and rectangular, as illustrated in Figure-4. Accurate measurements of length and radius are essential to ensure aerodynamic efficiency and structural integrity. Balsa wood is used and ideal for lightweight models. For economic purposes, PVC pipes are suitable for medium-sized constructions due to their durability for semi-circular slat and flaps.

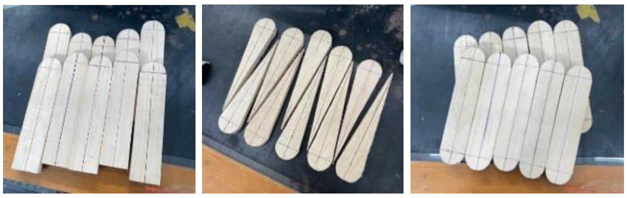

(a) (b) (c)

Figure-4. FWD Slat and AFT Flap design; (a) Rectangular, (b) Triangular, and (c) Semi-Circular.

Key structural design considerations include the spacing and number of ribs, which are connected to the spar with mortise joints for a secure fit and load distribution, strengthening the structure (Figure-5). Foam board is selected for the model's skin due to its flexibility and strength, and rib drilling ensures proper alignment for metal rod insertion. Carbon fiber, with its high strength-to-weight ratio, is used for the airframe in high-performance applications. The assembly is wrapped with a sticker for a polished finish and added protection, as shown in Figure-6.

(a) (b)

Figure-5. The ribs: (a) mortise joint for Rectangular and Semi-Circular; and (b) Metal rod inserts for Triangular slat and flap.

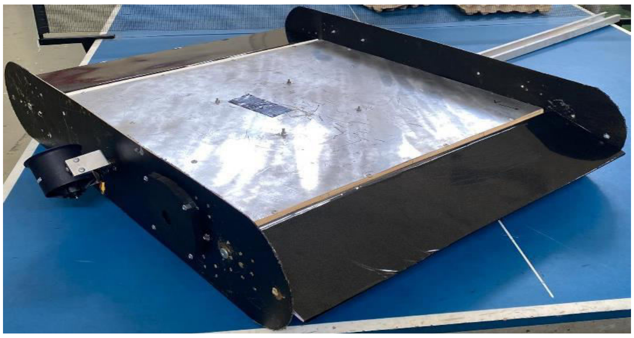

Figure-6. Assembled FWD slat and AFT flap embedment onto the Flat Plate experimental model.

2.2.2 Experimental setup

The experimental model was properly positioned within the OLWT testing area, mounted on a component balance in Figure-7. This balance stabilized the model and provided the flexibility to adjust its orientation, allowing for precise angle adjustment to suit a variety of test conditions. Accurate angle measurement was achieved using a digital protractor.

Figure-7. Component balance rig for experimental model.

A digital manometer played a critical role in assessing pressure variations within the wind tunnel. By detecting dynamic pressure exerted by the airflow, the manometer contributed significantly to estimating airspeed, which continuously monitored the tunnel's internal pressure at specific points, including the stagnation point, where airflow comes to rest against the model, and accurately determined the dynamic pressure. When combined with the known air density, these measurements were used to calculate airspeed, a crucial parameter for evaluating aerodynamic performance in the testing phases in OLWT, as shown in Figure-8.

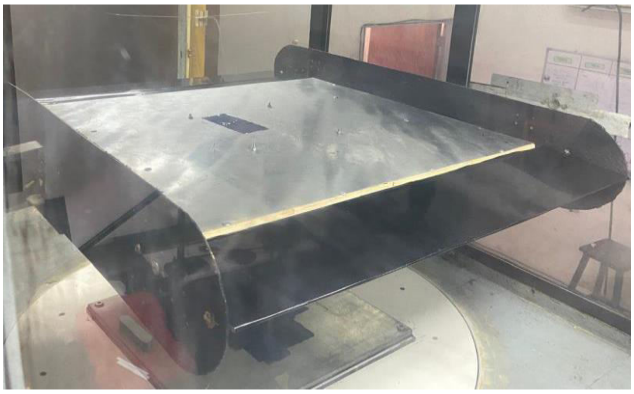

Figure-8. FWD slat and AFT flap embedment onto Flat Plate experimental model in Open Loop Wind Tunnel testing.

2.2.3 Open loop wind tunnel test procedures

The OLWT test procedures are essential for assessing aerodynamic performance by simulating airflow conditions around the test model illustrated in Figure-9. This process enables precise control of variables such as airflow velocity and angle of attack, allowing for accurate measurements of lift, drag, and pressure distribution, as outlined procedures shown in Figure-10. By attaching the model to a component balance and utilizing high-precision tools, data were systematically obtained on various flow conditions.

Figure-9. The Open Loop Wind Tunnel (Courtesy UPM-LST) with wind speed capacity is up to 50 ms^{-1} [17][20].

ISSN 1819-6608
ARPN Journal of Engineering and Applied Sciences

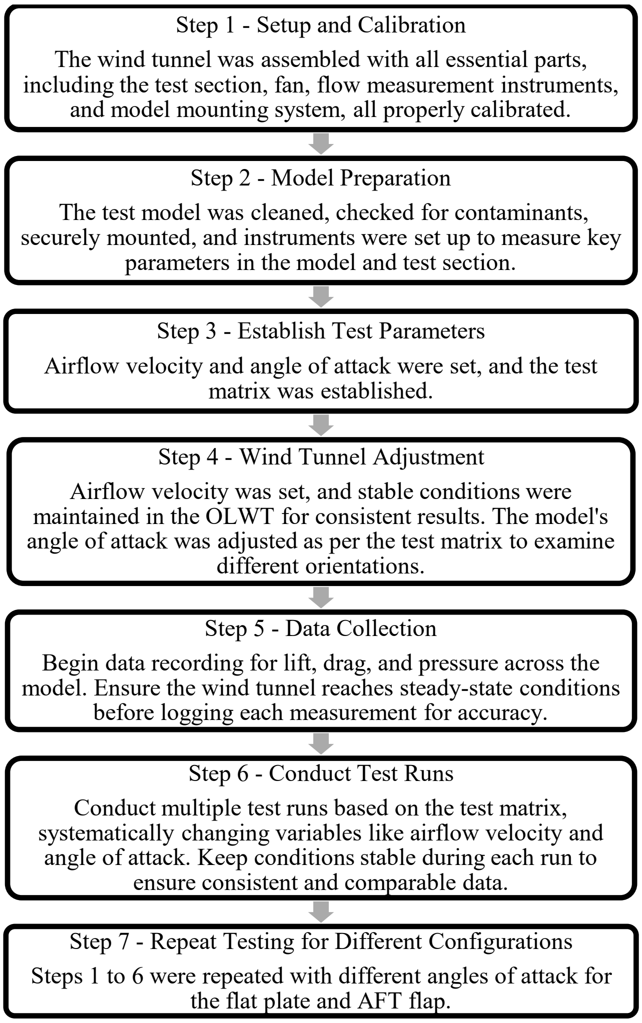

Figure-10. Semi-Active FWD (slat) and AFT (flap) embedment onto the Flat Plate experimental model in Open Loop Wind Tunnel testing procedures.

The angle of attack for each model configuration was measured and defined relative to the air velocity inlet direction, streamwise flow. The forward (FWD) air flow control, for each design variant, was held constant at a 0° angle of attack. Conversely, the central flat plate was tested at varying angles of attack set to 5° and 7° to observe incremental aerodynamic effects shown in Figure-11 as an example. The rear (AFT) air flow control of each design underwent a broader range of angle-of-attack variations of 0°, 5°, 10°, 15°, and 20° to assess its impact on performance under different deflection scenarios (Figure-11 and Table-1). This structured approach enabled the evaluation of each semi-active air flow control influence on the aerodynamic performance of multiple configurations. The experimental carried out for air inlet velocity at 5 ms^{-1} (Re = 2.9 x 10^5), 10 ms^{-1} (Re = 5.8 x 10^5), 15 ms^{-1} (8.7 x 10^5) and 20 ms^{-1} (1.2 x 10^6).

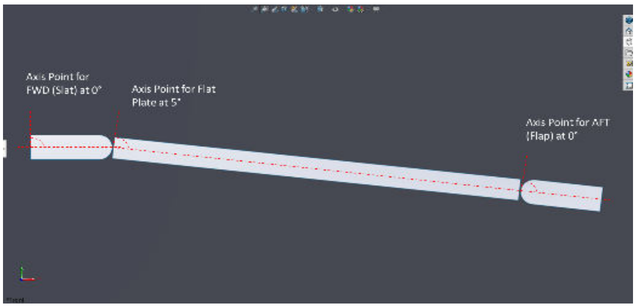

Figure-11. FWD (slat) at 0° and AFT (flap) at 0° (followed flat plate axis) embedment onto the Flat Plate at 5° experimental model in Open Loop Wind Tunnel testing procedures.

Table-1. Semi-Active Airflow Control: Rectangular, Triangular, and Semi-Circle Embedment onto Flat Plate Model Angle of Attack conditions.

Condition	FWD	Flat Plate	AFT
A	0°	5°	0°
B	0°	7°	0°
C	0°	7°	5°
D	0°	7°	10°
E	0°	7°	15°
F	0°	7°	20°

3. RESULTS

3.1 Aerodynamic Performance

The research measures lift, drag, pressure coefficient, and lift-to-drag ratio, aiming for high lift combined with low drag. An experiment was conducted in the OLWT, and the findings are discussed.

3.2 Experimental Analysis

In this research, the feasibility of the proposed configurations was assessed through experimental testing conducted in the OLWT to examine the lift, drag, pressure coefficient, and the lift-to-drag ratio. These parameters revealed patterns and relationships that characterize model performance under varying flow conditions, providing insight into how different configurations and velocities influenced the aerodynamic efficiency. This comparison is vital for optimizing design configurations aimed at maximizing lift and minimizing drag, thereby enhancing overall aerodynamic efficiency.

3.2.1 Effect on aerodynamic performance

In this study, velocity is treated as a vector quantity with specified input values at the velocity inlet. These input velocities were applied in the Reynolds number (Re) formula to predict fluid flow patterns, where velocity includes both direction and magnitude, while speed is the scalar value of velocity.

ARPN Journal of Engineering and Applied Sciences

As referred to Table-1, in the initial configuration (0°-5°-0°), a notable increase in airflow velocity was observed in the upper region. Subsequently, with the flat plate fixed at 7°, the aft flap was adjusted incrementally to 5°, 10°, 15°, and 20° to evaluate aerodynamic performance. Figure-12 illustrates the lift performance of a rectangular (a), triangular (b), and semi-circular (c) slat and flap configuration at various angles of attack over different air velocities from the experiment in OLWT.

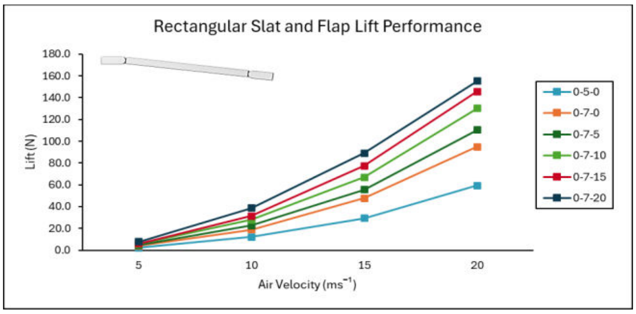

(a)

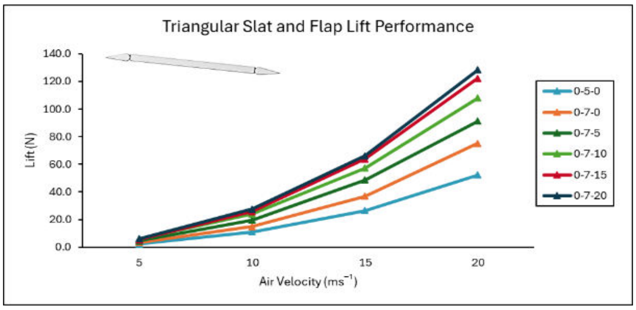

(b)

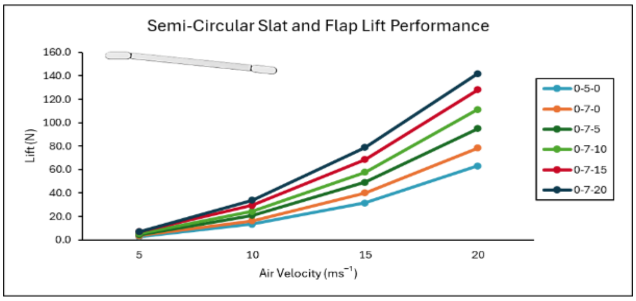

(c)

Figure-12. Lift performance: Rectangular (a), Triangular (b), and Semi-Circular (c) slat and flap embedment onto a flat plate experiment.

Notably, lift increases consistently with air velocity across all configurations and air flow control designs, demonstrating that higher velocities contribute positively to lift generation. The aft flap angle also plays a crucial role in lift enhancement; as the flap angle increases, particularly in configurations 0°-7°-10°, 0°-7°-15°, and 0°-7°-20°, lift values rise progressively. This trend suggests that greater flap deflection angles enhance lift by altering airflow patterns. The configuration with the highest lift output is 0°-7°-20°, achieving approximately 155.01 N for rectangular slat and flap, 128.47 N for triangular slat and flap, and 141.99 N for semi-circular slat and flap at 20 ms^{-1}, likely due to the combined effect of a steeper angle of attack and optimal flap positioning. Conversely, configurations with minimal aft flap deflection, such as 0°-5°-0°, yield lower lift and exhibit a moderate lift trend, indicating that limited flap deflection restricts lift performance for all slat and flap designs.

Figure-13 presents the drag performance of a rectangular (a), triangular (b), and semi-circular (c) slat and flap configuration. Generally, drag increases with air velocity across all configurations, indicating a direct relationship between velocity and drag forces. Configurations with higher aft flap angles, such as 0°-7°-10°, 0°-7°-15°, and 0°-7°-20°, show progressively higher drag values, reflecting the impact of increased flap deflection on drag.

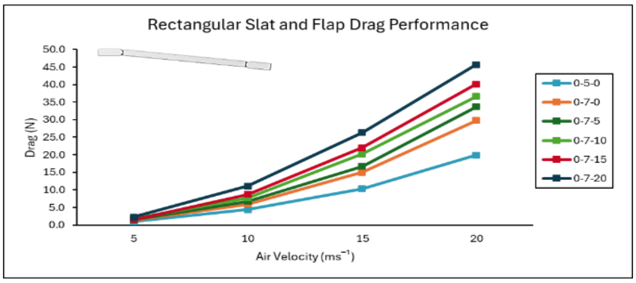

(a)

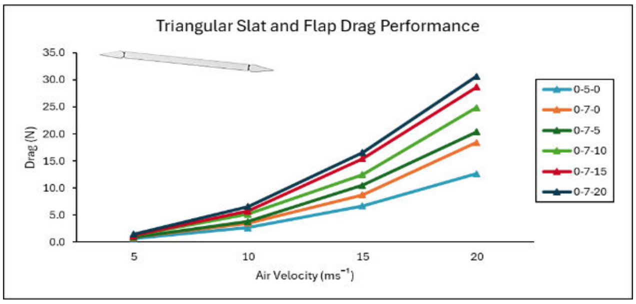

(b)

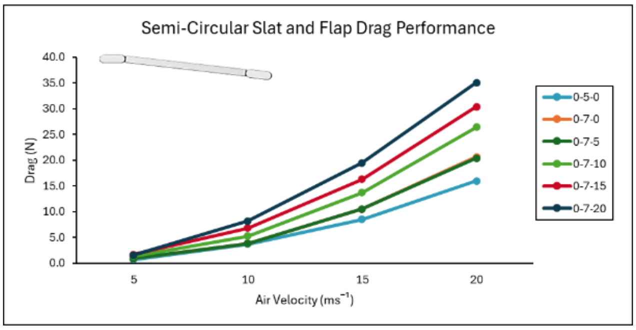

(c)

Figure-13. Drag performance: Rectangular (a), Triangular (b), and Semi-Circular (c) slat and flap embedment onto a flat plate experiment.

For instance, the 0°-7°-20° configuration generates the highest drag, reaching around 45.67 N for

ARPN Journal of Engineering and Applied Sciences

rectangular slat and flap, 30.69 N for triangular slat and flap, and 35.09 N for semi-circular slat and flap at 20 ms^{-1}, which suggests that large aft flap deflections amplify drag forces due to airflow disruption and increased surface resistance. Lower flap angle configurations, 0°-5°-0°, exhibit reduced drag, with values remaining lower across all velocities, highlighting the benefit of minimal deflection in drag reduction. This underscores the trade-off between lift and drag in aerodynamic optimization, as higher flap deflections, while beneficial for lift, simultaneously increase drag. Understanding this balance is crucial for optimizing the performance of the rectangular slat and flap configurations in practical applications.

Figure-14 illustrates the lift-to-drag ratio, $C_L/C_{D,}$ performance for a semi-circular slat and flap configuration for the tested model. The results demonstrate that most configurations maintain a relatively stable C_L/C_D across the velocity range, with values generally ranging between 2.310 and 5.161. Configurations with increased aft flap deflection exhibit slightly higher C_L/C_D ratios, reflecting optimized aerodynamic efficiency due to the balance of lift and drag forces. The 0°-0°-0° configuration shows an increasing trend in C_L/C_D as velocity rises, indicating improved aerodynamic performance at higher velocities, which stabilized at 10 ms^{-1} to 20 ms^{-1} despite its lower initial ratio. However, the 0°-7°-10° (all design) configurations consistently deliver high ratios. Meanwhile, the 0°-7°-15° (rectangular and semi-circular) configuration gave one of the highest ratios, suggesting it provides a favorable trade-off between lift and drag.

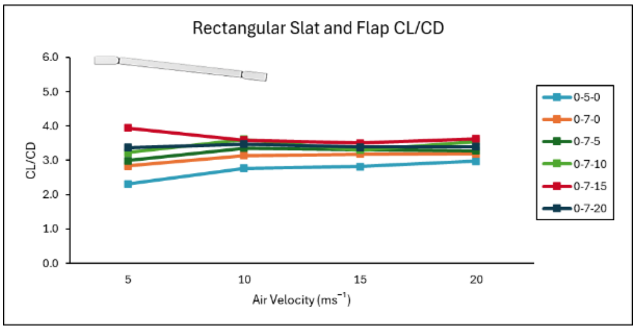

(a)

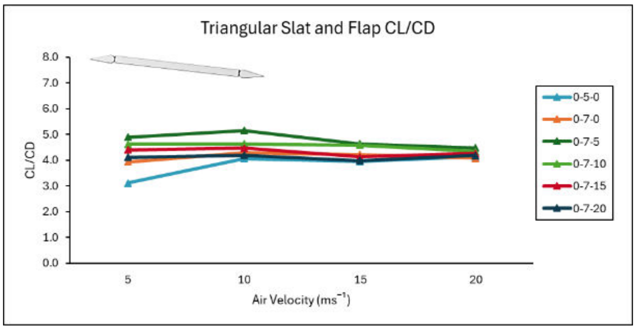

(b)

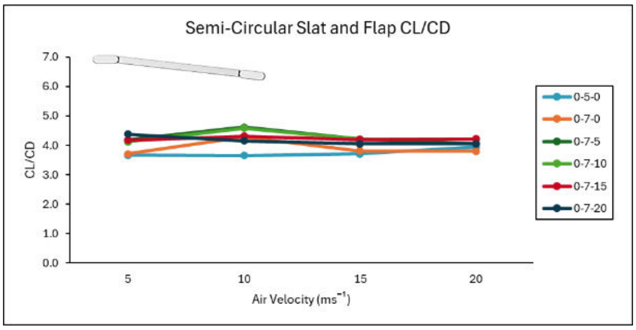

(c)

Figure-14. C_L/C_D; Rectangular (a), Triangular (b), and Semi-Circular (c) slat and flap embedment onto flat plate experiment.

Figure-15 illustrates a comparison of the aerodynamic performance between the AgroCyFlaP at a 5° pitch angle and the 0°-5°-0° slat and flap embedded flat plate configurations. The AgroCyFlaP exhibits higher C_L/C_D at low air velocities, achieving peak performance at 10 ms^{-1}. However, its efficiency declines sharply beyond this velocity, indicating its aerodynamic performance is optimized for low-speed operations. Conversely, the slat and flap embedded flat plate configurations (rectangular, triangular, and semi-circular designs) displayed stable and consistent C_L/C_D that increase with air velocity under the 0°-5°-0° configuration, outperforming the AgroCyFlaP. This suggests that these designs are better suited for high air velocity operations in terms of aerodynamic performance. The triangular slat and flap achieve the highest C_L/C_D at 4.134 for the air velocity of 20 ms^{-1}, demonstrating superior aerodynamic efficiency compared to the other designs. This result highlights the potential of the triangular slat and flap design for applications requiring high-speed performance and efficient lift-to-drag characteristics. Airflow in the wind tunnel was turbulent and unstable below 10 ms^{-1}, causing irregular patterns and inconsistent performance. Stability improved at 10 ms^{-1}, marking a critical threshold for reliable aerodynamic testing.

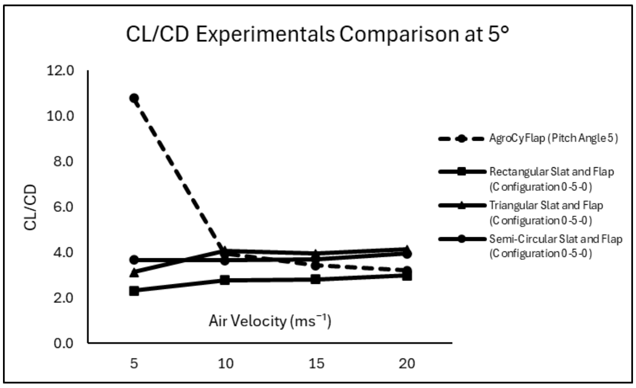

Figure-15. C_L/C_D comparison; AgroCyFlaP [9] to slat and flap embedment onto flat plate experiment at 5°.

ARPN Journal of Engineering and Applied Sciences

CONCLUSIONS

The study investigated the aerodynamic performance of various slat and flap configurations (rectangular, triangular, and semi-circular) embedded onto a flat plate model, focusing on their lift, drag, and lift-to-drag ratio (C_L/C_D) under different angles of attack and air velocities. Experimental results highlighted that lift performance consistently increased with air velocity across all configurations, with the aft flap angle significantly influencing lift generation. Among the tested designs, the 0°-7°-20° configuration yielded the highest lift, achieving 155.01 N for rectangular, 128.47 N for triangular, and 141.99 N for semi-circular configurations, respectively, at 20 ms^{-1}. However, higher flap deflections also increased drag forces, with the same configuration producing maximum drag values of 45.67 N for rectangular, 30.69 N for triangular, and 35.09 N for semi-circular, demonstrating a trade-off between lift enhancement and drag amplification.

The C_L/C_D analysis revealed that while the AgroCyFlaP performed better at low velocities (≤10 ms^{-1}), its efficiency sharply declined at higher velocities, limiting its suitability for high-speed applications. In contrast, the slat and flap configurations displayed stable and consistent C_L/C_D values, particularly under the 0°-0°-0° and 0°-5°-0° configurations, compared with the AgroCyFlaP, with the triangular design achieving the highest C_L/C_D of 4.134 at 20 ms^{-1}. These findings underscore the superior aerodynamic efficiency of the triangular configuration for high-speed operations.

Slat and flap configurations present a promising alternative to the AgroCyFlaP model, addressing its aerodynamic limitations at higher velocities. Experimental analyses demonstrate that triangular and semi-circular designs achieve superior lift-to-drag ratios and enhanced stability across diverse flight conditions. These configurations should minimize mechanical load, reduce power consumption, and decrease overall UAV HAP system weight, thereby improving design efficiency.

The study concluded, slat and flap embedded flat plate designs, particularly the triangular and semi-circular configurations, are well-suited for UAV High-Altitude Platform (HAP) systems application, offering high efficiency and optimized aerodynamic performance. This advancement supports lightweight, energy-efficient designs for future HAP applications.

REFERENCES

[1] F. A. D'Oliveira, F. C. L. De Melo and T. C. Devezas. 2016. High-altitude platforms - Present situation and technology trends. J. Aerosp. Technol. Manag., 8(3): 249-262, doi: 10.5028/jatm.v8i3.699.

[2] J. N. Pelton and S. Madry. 2018. Handbook of Small Satellites. doi: 10.4324/9781351181846.

[3] T. E. Noll, J. M. Brown, M. E. Perez-Davis, S. D. Ishmael, G. C. Tiffany, and M. Gaier. 2004. Investigation of the Helios Prototype Aircraft Mishap. Vol. I Mishap Rep. I(January): 100.

[4] NASA - Helios. Accessed: Sep. 18, 2022. [Online]. Available: https://www.nasa.gov/centers/dryden/news/ResearchUpdate/Helios/

[5] M. S. Alias, A. S. M. Rafie, M. F. A. Hamid, E. Gires, and K. D. M. Aris. 2024. Wind Profiles in Peninsular Malaysia: A Comprehensive Upper Air Analysis. Sains Malaysiana, 53(3): 487-499, doi: 10.17576/jsm-2024-5303-02.

[6] H. M. Ali, A. S. M. Rafie, S. A. M. Ali, and E. Gires. 2021. Computational Analysis of the Rotating Cylinder Embedment onto a Flat Plate. CFD Lett., 13(12): 133-149, doi: 10.37934/cfdl.13.12.133149.

[7] H. M. Ali. 2022. Aerodynamic Analysis on Cylinder to Flat Plate Embedment for High Altitude Platform Station Application. Univ. Putra Malaysia, vol. Ph.D. theses. (December).

[8] A. M. Mgaidi, A. S. Mohd. Rafie, K. A. Ahmad, R. Zahari, M. F. Abdul Hamid, and O. F. Marzuki. 2018. Numerical and experimental analyses of the flow around a rotating circular cylinder at a subcritical regime of Reynolds number using K-E and K-Ω-SST turbulent models. ARPN Journal of Engineering and Applied Sciences. 13(3): 954-960.

[9] S. W. Azman, A. S. M. Rafie, and E. Gires. 2024. Aerodynamic Analysis of Cylinder to Flat Plate (CyFlap) Embedment for Agriculture Purposes. J. Aeronaut. Astronaut. Aviat., 6(1): 357-364, doi: 10.6125/JoAAA.202403_56(1S).24.

[10] J. D. Anderson. 1989. Introduction to Flight, 3rd Edition.

[11] J. Wang and L. Feng. 2018. Introduction. Flow Control Tech. Appl., pp. 1-22, doi: 10.1017/9781316676448.002.

[12] J. J. Wang, Y. C. Li, and K. S. Choi. 2008. Gurney flap-Lift enhancement, mechanisms and applications. Prog. Aerosp. Sci., 44(1): 22-47, doi: 10.1016/j.paerosci.2007.10.001.

[13] M. Gad-el-Hak. 2001. Flow control: The future. J. Aircr., 38(3): 402-418, doi: 10.2514/2.2796.

[14] S. C. McParlin, R. J. Bruce, A. G. Hepworth, and A. J. Rae. 2006. Low speed wind tunnel tests on the 1303 UCAV concept. Sr. Memb. AIAA † Princ. Sci. (8): 1-17.

[15] M. T. Boyle. Low Speed Wind Tunnel Testing. pp. 31-39.

[16] D. Greenblatt. 2016. Unsteady Low-Speed Wind Tunnels. AIAA J., 54(6): 1817-1830, doi: 10.2514/1.J054590.

[17] S. Wiriadidjaja, F. Hasim, S. Mansor, W. Asrar, A. S. M. Rafie, and E. J. Abdulla. 2012. Subsonic wind tunnels in Malaysia: A review. Appl. Mech. Mater., 225: 566-571, doi: 10.4028/www.scientific.net/AMM.225.566.

[18] T. J. Mueller and G. E. Torres. 2001. Aerodynamics of Low Aspect Ratio Wings at Low Reynolds Numbers with Applications to Micro Air Vehicle Design and Optimization. Security, no. November, p. 112, 2001.

[19] E. S. Aziz, C. Chassapis, S. Esche, S. Dai, S. Xu, and R. Jia. 2008. Online Wind Tunnel Laboratory. ASEE Annu. Conf. Expo. Conf. Proc., (March 2015), doi: 10.18260/1-2--3402.

[20] O. F. Marzuki, A. S. Mohd Rafie, F. I. Romli and K. A. Ahmad. 2015. An experimental investigation on the effect of surface roughness on the performance of the Magnus wind turbine. ARPN J. Eng. Appl. Sci., 10(20): 9725-9729.